IMAGE-BASED CONSTRUCTION OF LUNAR DIGITAL ELEVATION MODELS OF VERY HIGH LATERAL RESOLUTION. A. Grumpe[1] and C. Wöhler[1], [1]Image Analysis Group, TU Dortmund University, D–44227 Dortmund, Germany; {arne.grumpe | christian.woehler}@tu-dortmund.de

Introduction: Lunar digital elevation models (DEMs) of high lateral resolution are used for a variety of applications, ranging from the calibration of multispectral data [1] to the automatic detection of craters [2]. Unfortunately, the lateral resolution of available DEMs does not meet the requirement of pixelsynchronous imagery and topographic maps. This abstract describes a method to create DEMs of high lateral resolution from imagery of high lateral resolution and DEMs of lower lateral resolution.

Available DEMs: The most recently published lunar DEMs are the Lunar Orbiter Laser Altimeter (LOLA) DEM [3] and the GLD100 DEM [4]. However, the gridded LOLA DEM (cf. Fig. 1a) suffers from interpolation gaps and does not reach the lateral resolution of current hyperspectral imagery, such as the Chandrayaan-1 M³ imagery with its typical resolution of 140 m/pixel (http://m3.jpl.nasa.gov/m3data.html). The GLD100 is a DEM which has been constructed based on stereophotogrammetric analysis of LROC WAC images and has a nominal lateral resolution of 100 m/pixel. However, it is shown in Fig. 1b that the GLD100 misses small craters which are well visible in the M³ data and therefore has an effective lateral resolution well below the nominal one (cf. Fig 1d). Previously, we have published a DEM refinement scheme based on a shape from shading (SfS) algorithm and an extended photoclinometry (PHCL) scheme [5].

Analysing the SfS solution: The original DEM construction method is divided into two parts:

1. The surface gradients *p* and *q* are estimated using an initial surface estimate and an image.
2. A surface *z* is found that fits the usually nonintegrable gradient estimates *p* and *q* by minimising $J = 1/2 \iint (\partial z/\partial x - p)^2 + (\partial z/\partial y - q)^2$

This approach leads to a Poisson equation in *z*. In order to estimate *z*, a discrete approximation of the Laplace operator is made, involving an average over the neighbouring pixels. This introduces a kind of low-pass filter and explains why the estimated surface (Fig. 1c) appears to be slightly blurred.

In order to avoid the undesirable blur, another surface estimate may be obtained using the PHCL to determine the surface gradient estimates *p* and *q* and use the Poisson solver described in [6] to compute the surface. The result (cf. Fig. 2a) displays a higher lateral resolution in terms of visible craters, but artifacts are introduced that may be due to inaccurate albedo estimation or image noise affecting the gradients. These effects appear to be suppressed by the low-pass filter of the method described in [5].

Modifying the SfS scheme: The original SfS problem is reformulated to incorporate a deviation of the estimated surface from a known DEM, which constrains the solution to be close to the known DEM.

Adding a constraining DEM. Since the available DEMs commonly do not share the lateral resolution of the imagery, the deviation of the estimated DEM from the constraining DEM is computed on a lower scale:

$$J = 1/2 \iint (\partial z/\partial x - p)^2 + (\partial z/\partial y - q)^2 + \sigma\, 1/2 \iint (f(z) - f(z_{DEM}))^2$$

where z_{DEM} denotes the constraining DEM and $f(x)$ is an arbitrary low-pass filter function and σ a weight factor. From the calculus of variations, the Euler equation

$$F = -\sigma(f(z) - f(z_{DEM}))\frac{\partial}{\partial z} f(z) - \frac{\partial}{\partial x} p - \frac{\partial}{\partial y} q + \Delta z = 0$$

follows, which requires the partial derivative $\partial/\partial z\, f(z)$ of the low-pass filter function.

Computing the partial derivative. Within this study $f(z) = G * z$ is assumed to be a convolution with a Gaussian low-pass filter *G*. The partial derivative can be computed using the chain rule according to

$$\partial/\partial x\, f(z) = \partial/\partial z\, f(z) \cdot \partial z/\partial x = G * (\partial z/\partial x)$$
$$\partial/\partial y\, f(z) = \partial/\partial z\, f(z) \cdot \partial z/\partial y = G * (\partial z/\partial y)$$

Although both formulations are mathematically identical, numerical inaccuracies are to be expected and both equations are solved in a least-squares approach:

$$\partial/\partial z\, f(z) = \frac{\partial z/\partial x \cdot \partial/\partial x\, f(z) + \partial z/\partial y \cdot \partial/\partial y\, f(z)}{(\partial z/\partial x)^2 + (\partial z/\partial y)^2}$$

The singularity at $\partial z/\partial x = \partial z/\partial y = 0$ is not treated specifically as it does not occur in the regarded examples.

Solving the Euler equation. The solution of the Euler equation is computed by randomly changing the surface at the point (x_r, y_r) to $z(x_r, y_r) \leftarrow z(x_r, y_r) + \varepsilon$. If the absolute value of *F* decreases, the step is accepted. Otherwise, $z(x_r, y_r) \leftarrow z(x_r, y_r) - \varepsilon$ is tested. If both changes are neglected, the point (x_r, y_r) is removed from the list of admissible points, where intially all points are admissible. Upon reaching an empty list of admissible points, the stepsize is reduced to $\varepsilon \leftarrow \varepsilon/2$ and all points become admissible again. This is repeated until the stepsize ε is sufficiently small.

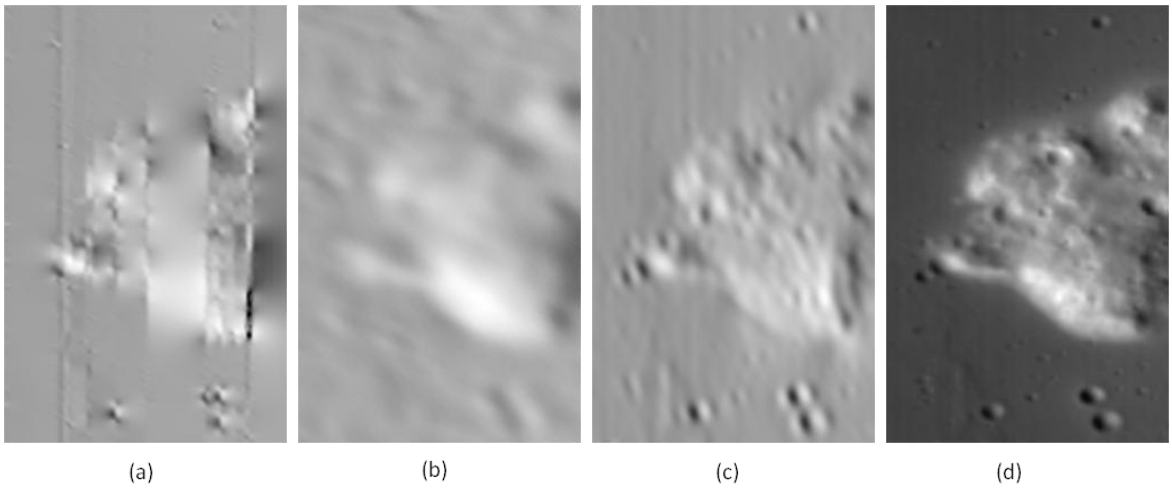

Fig. 1: Shaded views of the Mairan "middle" highland dome. (a) LOLA DEM. (b) GLD100. (c) DEM obtained with the method described in [5]. (d) M^3 image of the same region. All DEMs were shaded for the illumination conditions of the M^3 image using the Hapke IMSA model [7, 8, 9] with a uniform single-scattering albedo.

Results: As a test region we regarded the highland dome Mairan "middle". The Hapke IMSA model [7, 8, 9] was used for DEM construction. In the newly obtained DEM shown in Fig. 2b, small craters are visible which can barely be seen in the DEM constructed using the method described in [5] (cf. Fig. 1c). Although these craters appear in the DEM constructed with the Poisson solver [6], they are more pronounced in the new DEM, i.e. their depths are larger.

At the southwestern rim of Mairan "middle", the transition from the high-albedo volcanic material to the lower-albedo mare surface is rather sharp, which influences the surface gradients obtained with the method described in [5] and results in a rille-like artifact in the surface (cf. Fig. 2a). This artifact is less pronounced in the new DEM. Furthermore, the boundary conditions assumed by the Poisson solver [6] lead to artifacts, e.g. the steep southeastern flank of the mountain. This behaviour is not reproduced by our method, which does not enforce specific boundary conditions.

Conclusion: In this study, we have shown that the proposed algorithm can be used to increase the lateral resolution of DEMs constructed using image-based photometric methods. On large spatial scales, the obtained DEM is constrained by a known DEM of lower lateral resolution. It is not affected by boundary conditions and exhibits a very high lateral resolution.

References: [1] Hicks M. D. et al. (2011) *J. Geophys. Res. 11*, E00G15. [2] Boardman et al. (2011) *J. Geophys. Res. 116*, E00G14. [3] Smith D. E. et al (2010) *LPSC XLI*, abstract #1993. [4] Scholten F. et al (2011) *LPSC XLII*, abstract #2046. [5] Grumpe A. et al. (2011) *Proc. 7th Int. Symp. Image and Signal Processing and Analysis*, 609–614. [6] Simchony T. et al. (1990) *TPAMI 12*, 435–446. [7] Hapke B. W. (1981) *J. Geophys. Res. 86*, 3039–3054. [8] Hapke B. W. (1984) *Icarus 59*, 41–59. [9] Hapke B. W. (1986) *Icarus 67*, 264–280.

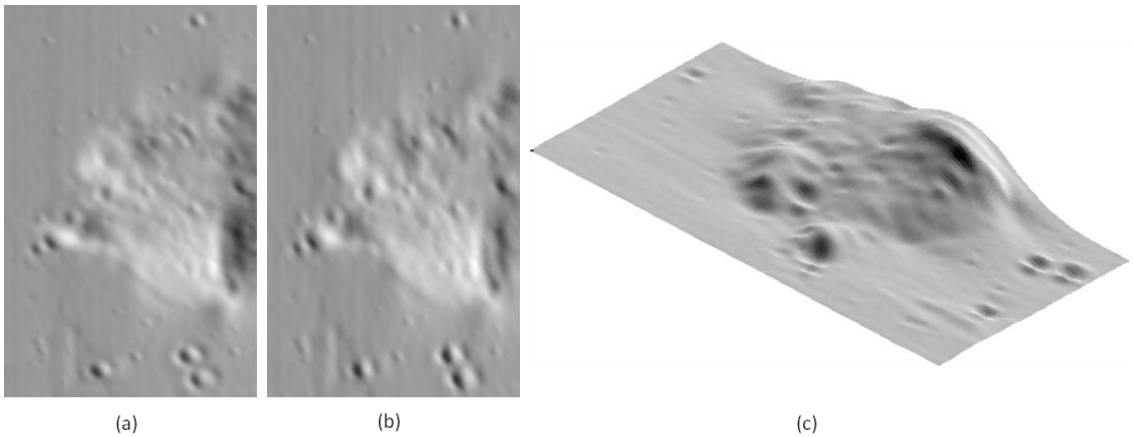

Fig. 2: Constructed DEMs (shaded as in Fig. 1). (a) Result of the Poisson solver desribed in [6]. (b) Result of the method proposed in this study. (c) Perspectivical view of the result of the method proposed in this study. The vertical axis is five times exaggerated. The diameter of the dome corresponds to 9 km.